Lithospheric modeling in Iran from gravity and magnetic data including seismic tomographic data: first results.

Gerardo Maurizio[1], Carla Braitenberg[1], Daniele Sampietro[2], and Martina Capponi[2]

1. Trieste University Trieste University, Dept. of Mathematics and Geosciences, Italy
2. Geomatics Research & Development srl, Lomazzo, Italy

to PICO presentation

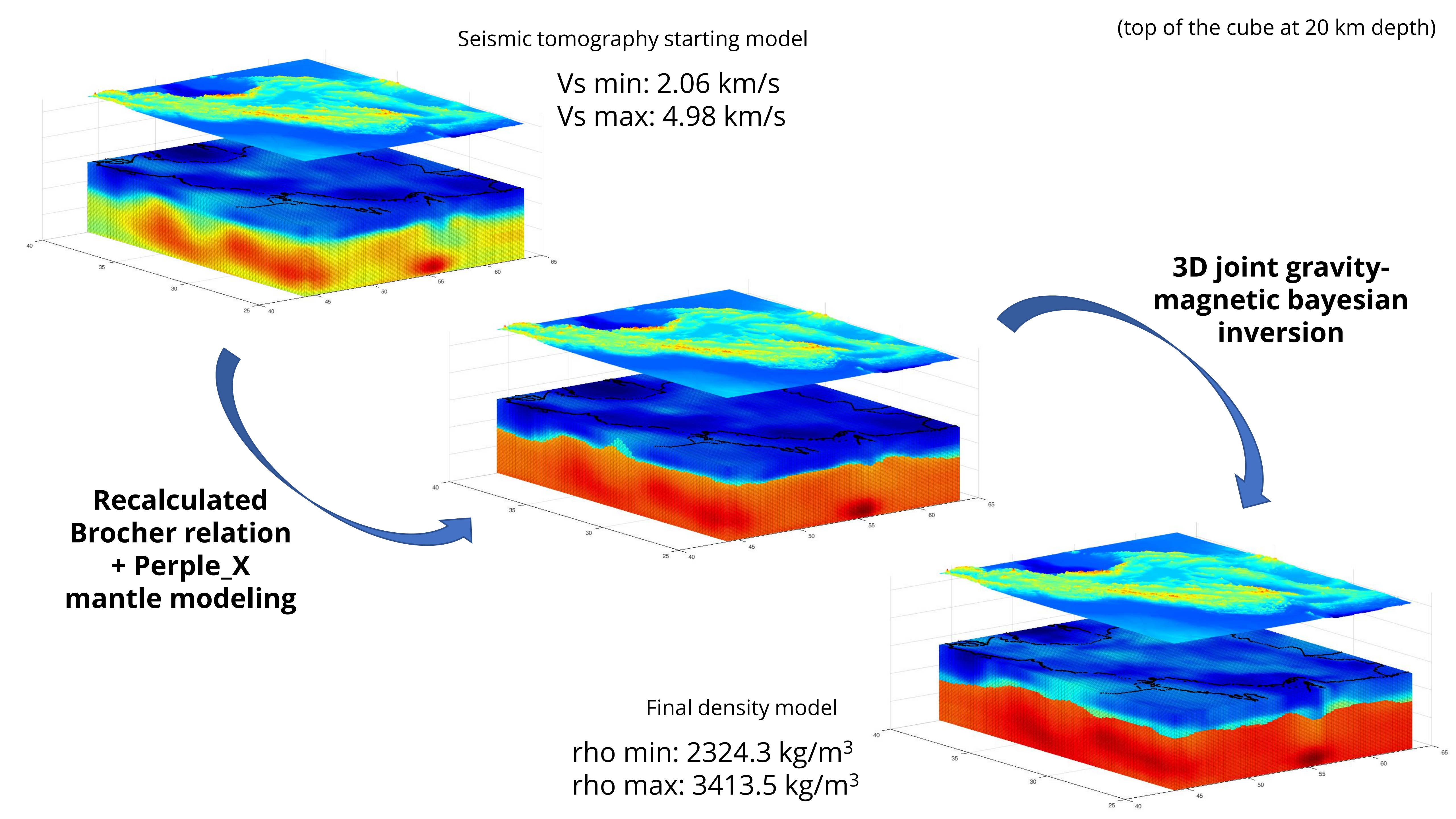
(top of the cube at 20 km depth)
Seismic tomography starting model
Vs min: 2.06 km/s
Vs max: 4.98 km/s
3D joint gravity-magnetic bayesian inversion
Recalculated Brocher relation + Perple_X mantle modeling
Final density model
rho min: 2324.3 kg/m3
rho max: 3413.5 kg/m3

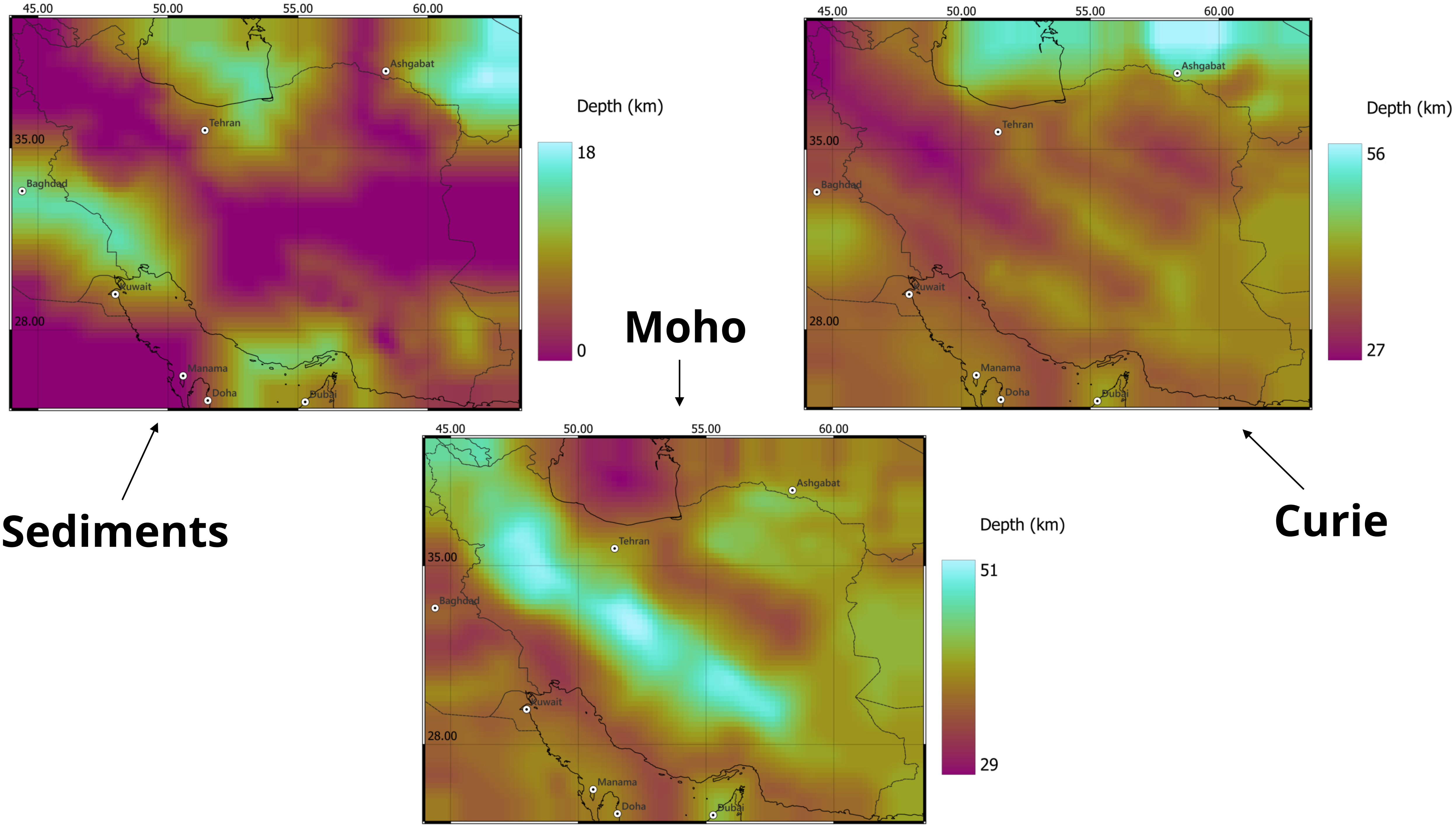
Sediments
Moho
Curie
Depth (km)
18
0
Depth (km)
56
27
Depth (km)
51
29
45.00
50.00
55.00
60.00
35.00
28.00
Ashgabat
Tehran
Baghdad
Kuwait
Manama
Doha
Dubai

- Inverted (density and susceptibility) and calculated (shear modulus) models
- (slice at at 20 km depth)

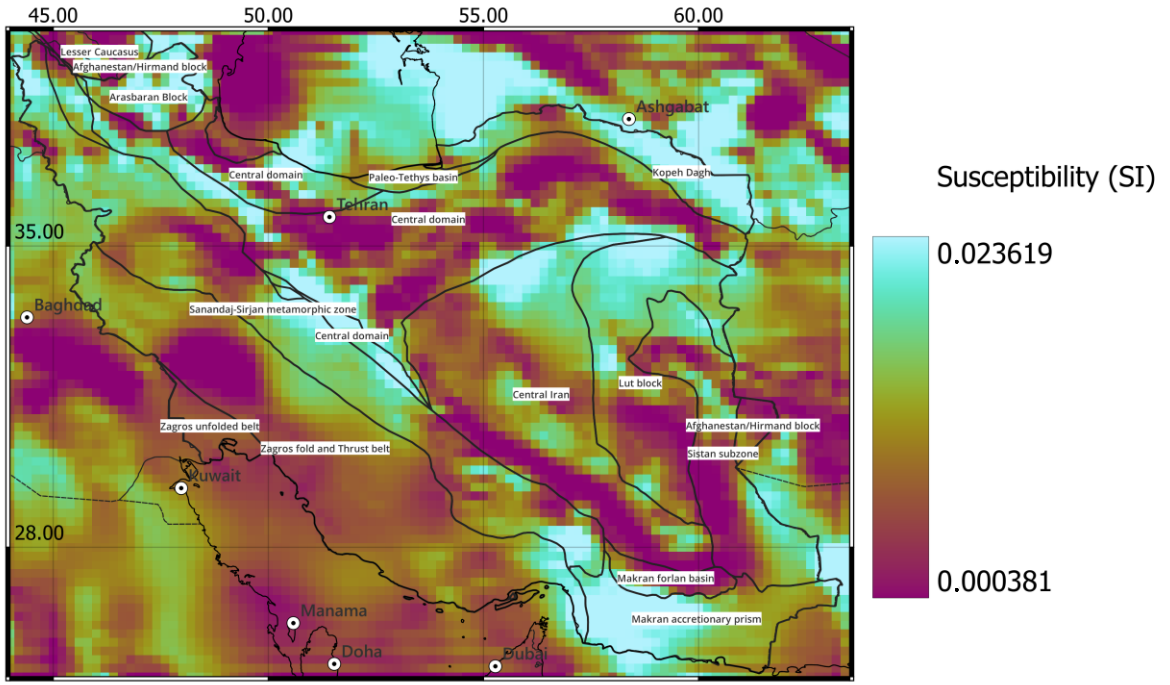

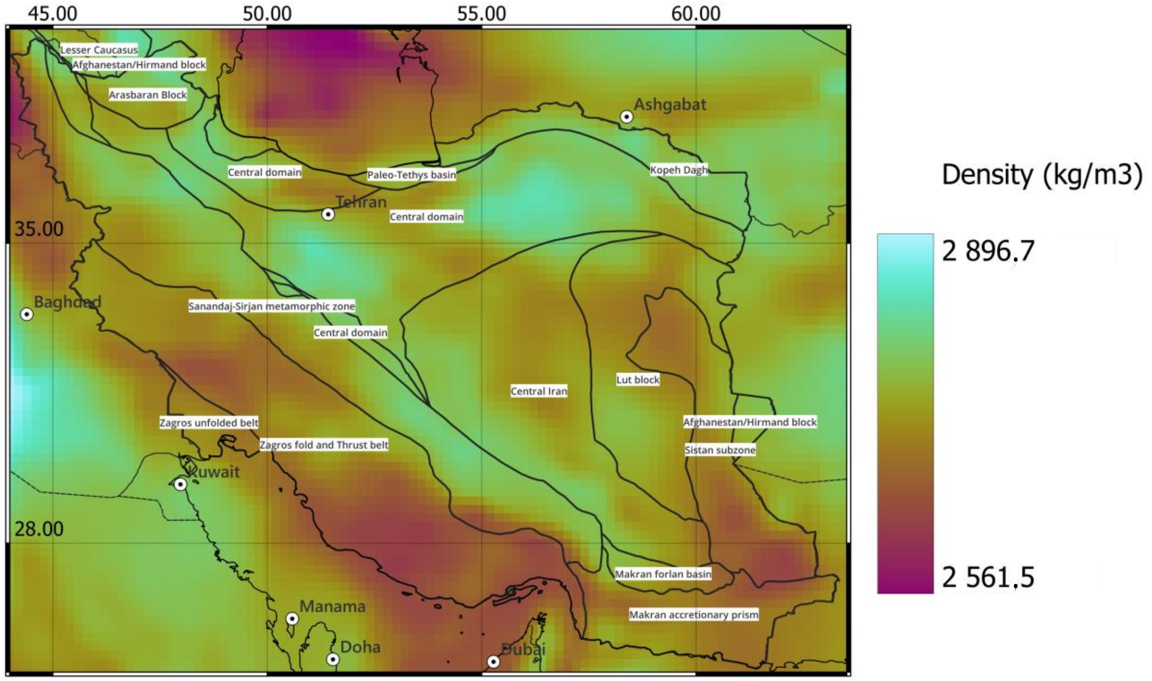

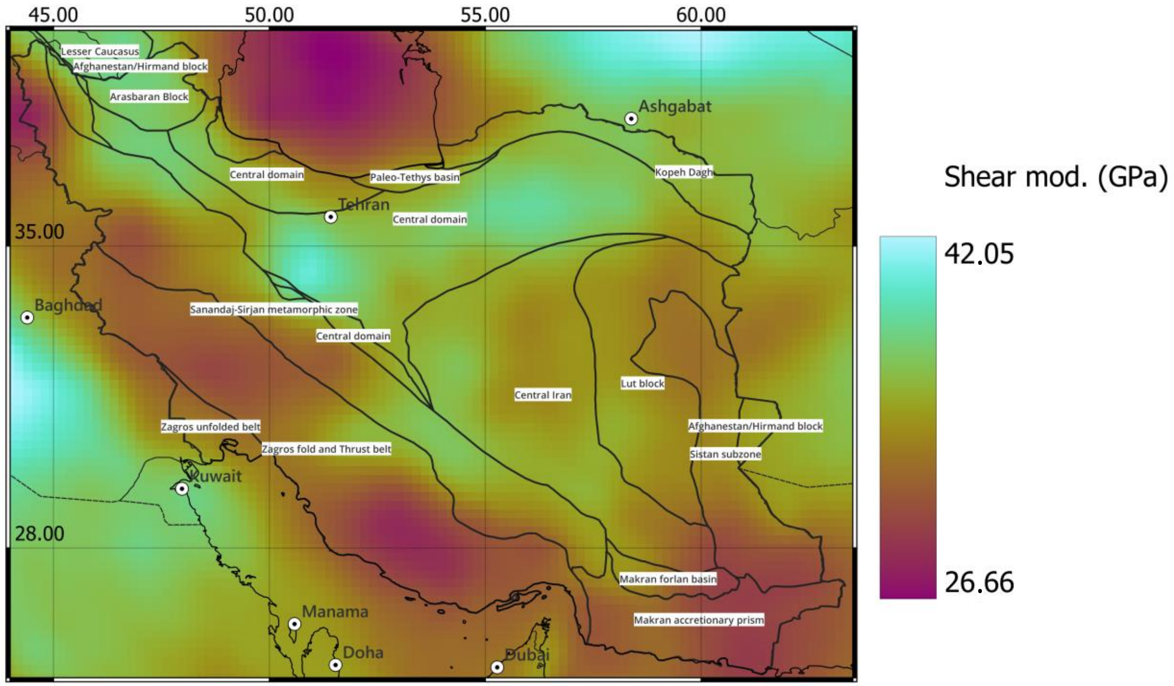

PICO presentation

Interactive outline

1. Geological introduction

3. Conversion formula

2. Datasets used

4. Results & Conclusion

Tectonic setting

Iranian plateau: zone of continental deformation formed by the Arabian-Eurasian collision (25 Ma).

Evolution associated to opening and closure of Paleo- and Neo-Tethys oceans.

Iranian plateau formed with the coalescing of island-arcs and continental fragments of Gondwana.

Closing of Neo-Tethys and Arabian-Eurasian collision began in early Miocene.

Northward motion of Arabian plate formed the Zagros Fold Belt and Iranian Plateau NE of Bitlis-Zagros suture.

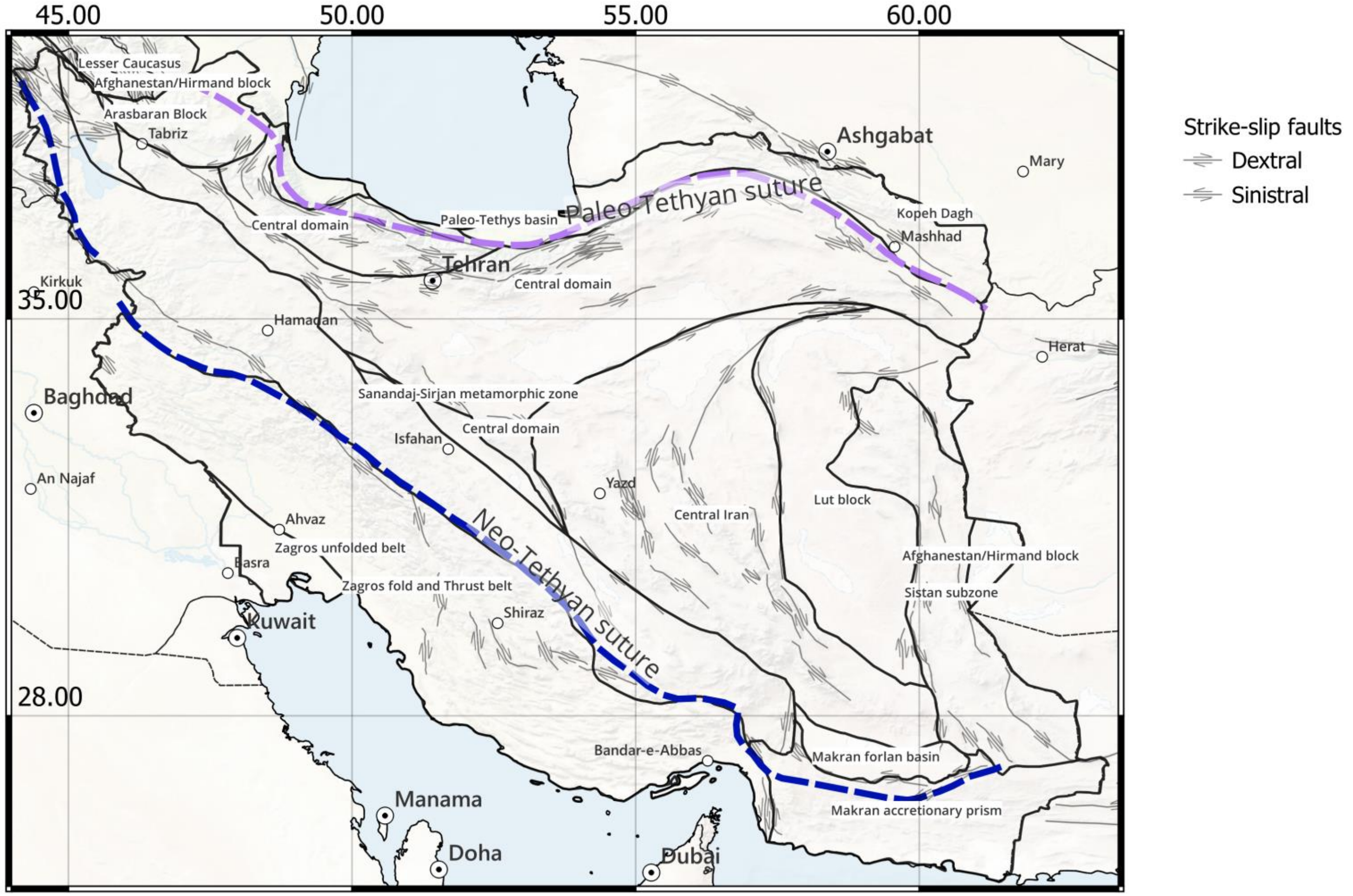

Iranian magmatism

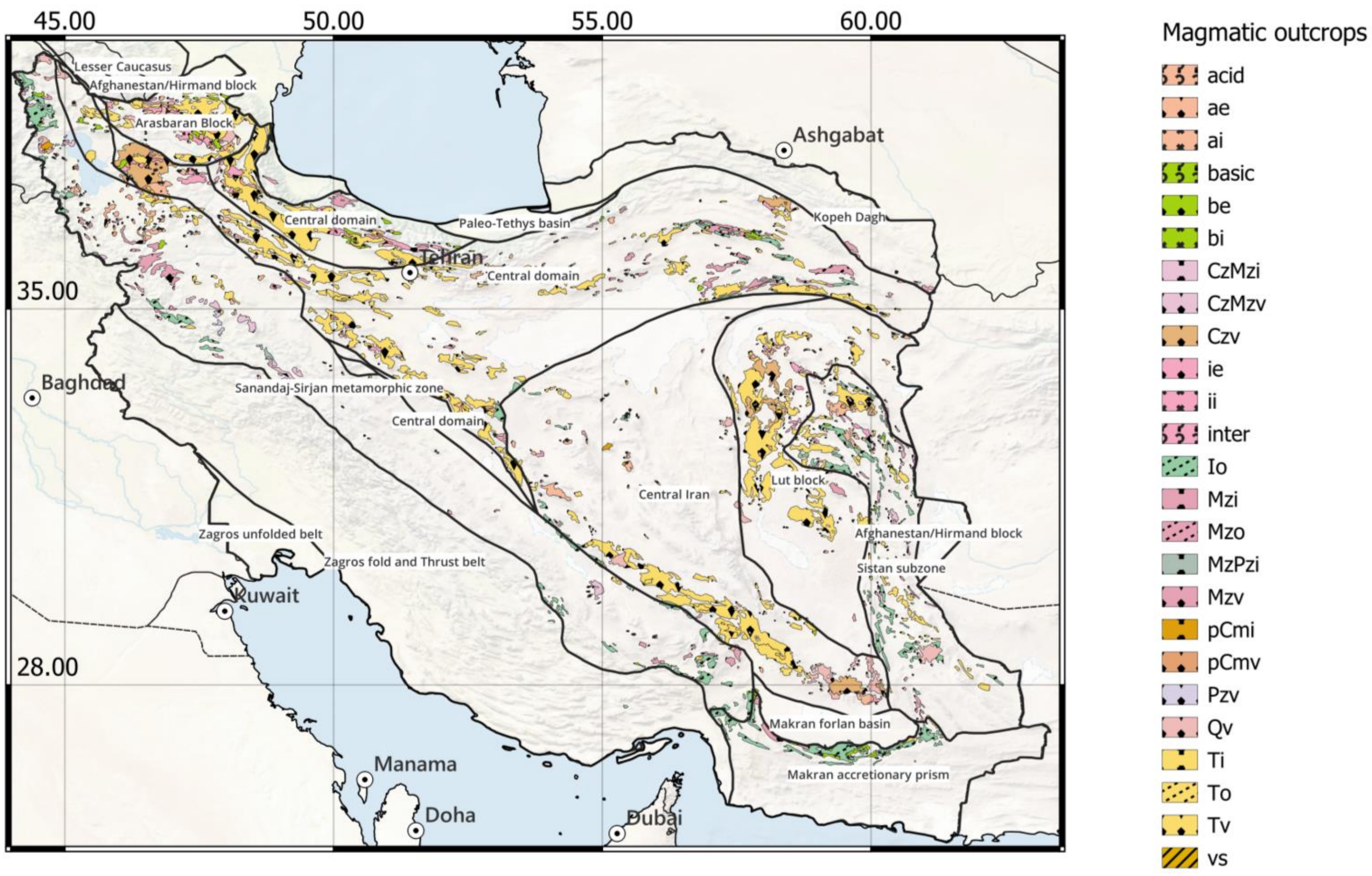

*Urumieh Doktar magmatic arc (UDMA) is a magmatic outcrops area across Iran from NW to SE, parallel to Zagros belt

- Major volcanism in the area is Tertiary (along UDMA*, in the Lut block, and in the Central Domain following the principal tectonic lineaments).
- Mesozoic volcanism is also relevant, mainly in the north-west of the area, close to Urmia lake.
- Ophiolites outcrop in the Makran area and in Sistan subzone

Datasets used

- Seismic tomography (Kaviani et al., 2020)

Seismic tomography Resolution:

Spatial Resolution = 0.25° (~27 km)
Vertical Resolution = 1 km to 7 km

Final Cube dimension (76x98x75):

Latitude = 25 ÷ 40 °N;
Longitude = 44 ÷ 63.4 °E;
Depth max = 105 km

We conserve vertical resolution from seismic original model. Final spatial resolution is 0.2° (~22 km)

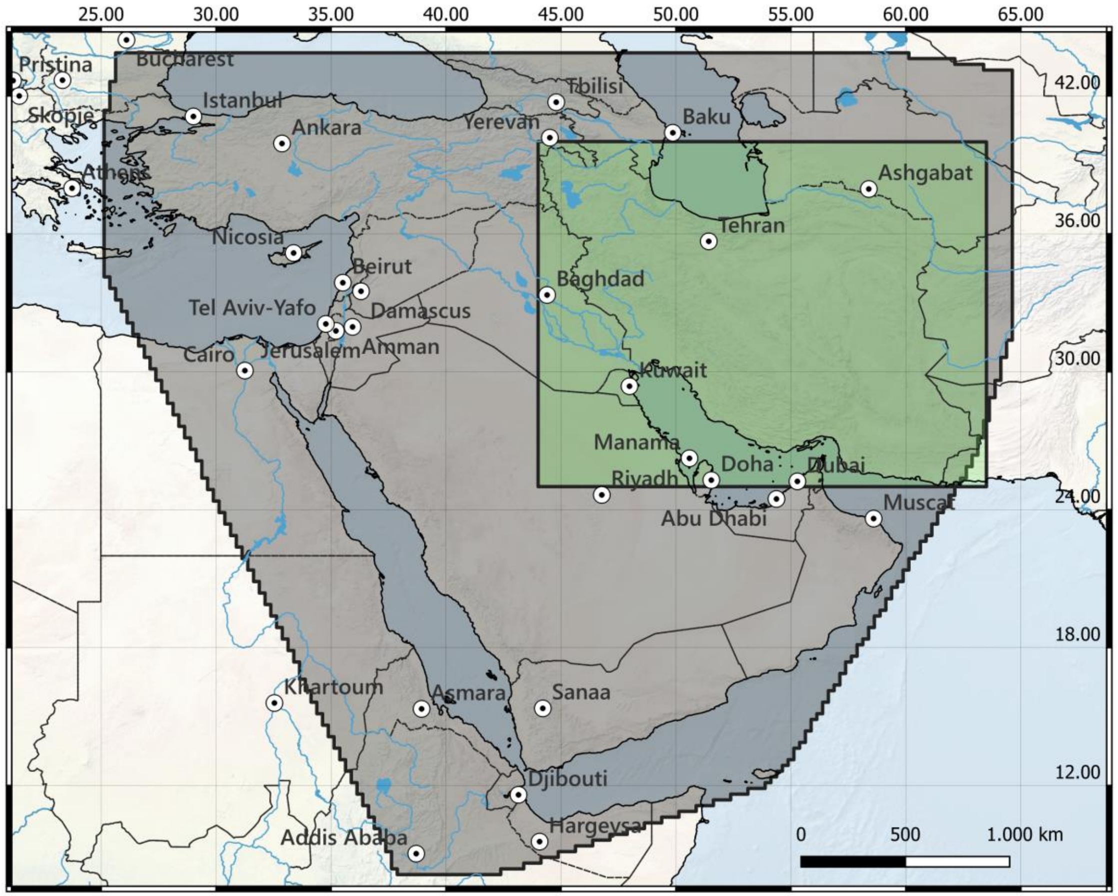

Area covered by the regional tomography (black area). Green box is the area selected for this work.

- Kaviani et al., 2020, *Crustal and uppermost mantle shear wave velocity structure beneath the Middle East from surface wave tomography.* Geophysical Journal International, 221(2), 1349-1365.

- Zingerle, P., Pail, R., Gruber, T. *et al.* The combined global gravity field model XGM2019e. *J Geod* **94**, 66 (2020). https://doi.org/10.1007/s00190-020-01398-0

- Brian Meyer; Richard Saltus; and Arnaud Chulliat. 2017: EMAG2v3: Earth Magnetic Anomaly Grid (2-arc-minute resolution). Version 3. NOAA National Centers for Environmental Information. https://doi.org/10.7289/V5H70CVX

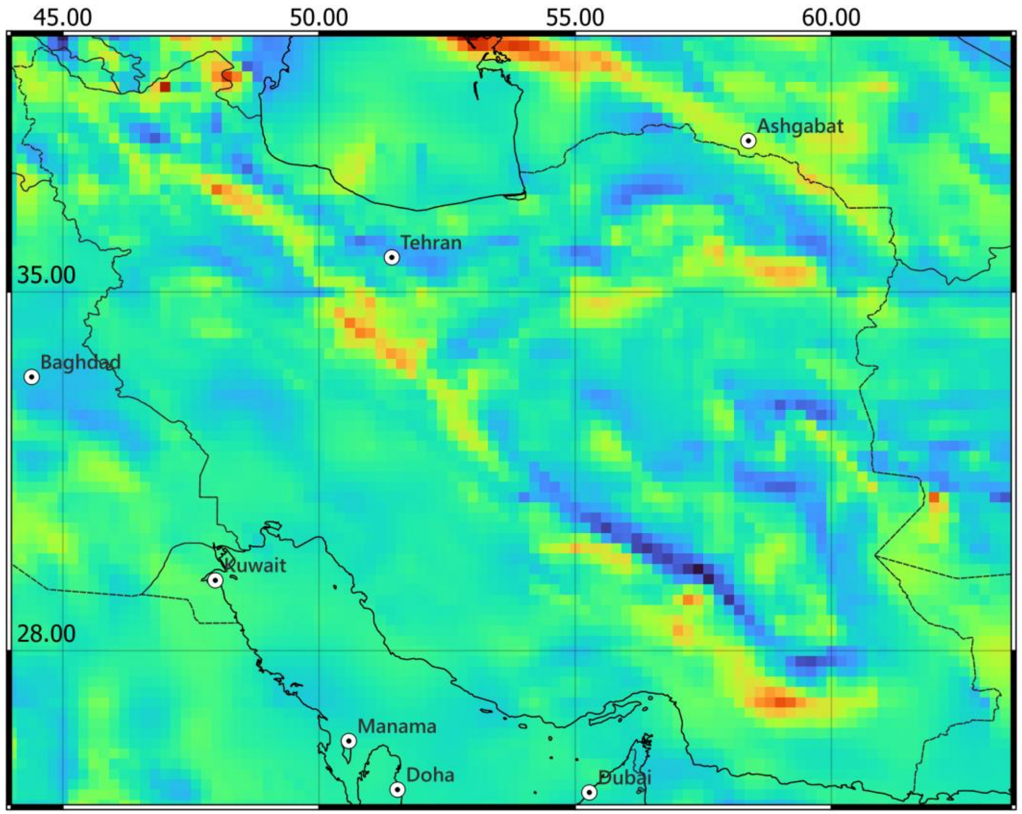

Magnetic observation (EMAG2 v3, measured at 4 km continuous altitude upon continents)

Gravity observation (XGM2019e, reduced by lower degree < 12)

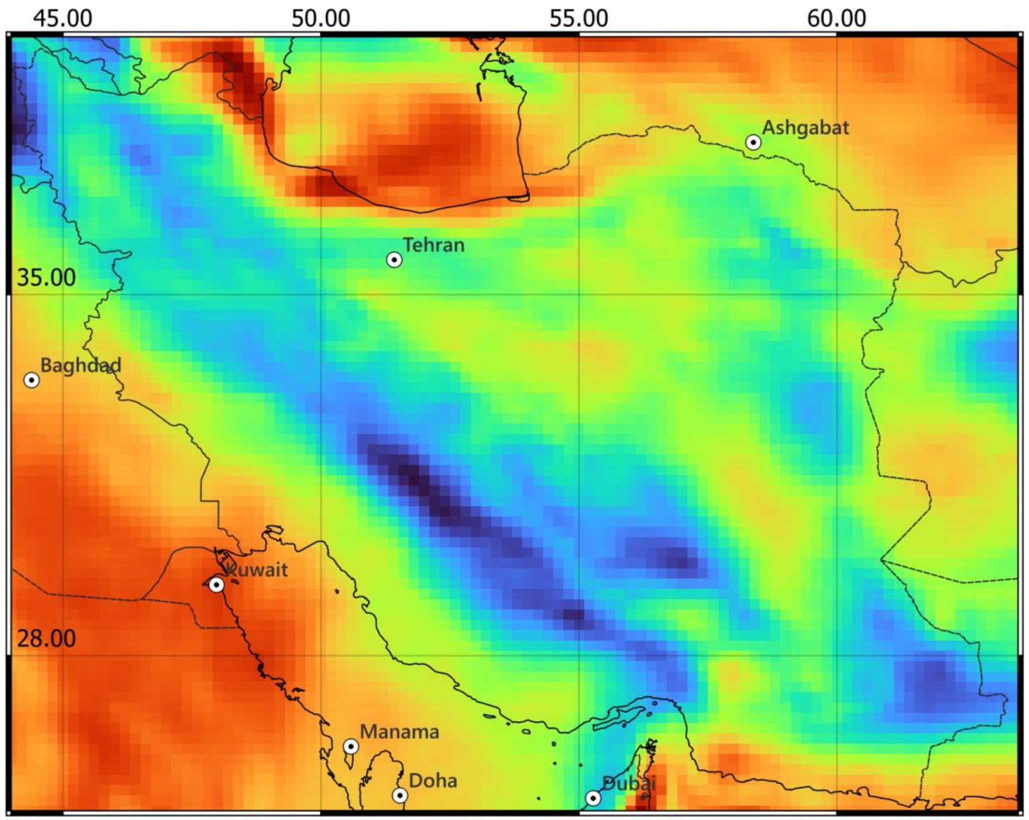

- Irandoust, M. A., Priestley, K., & Sobouti, F. (2022). High-resolution lithospheric structure of the Zagros collision zone and Iranian Plateau. Journal of Geophysical Research: Solid Earth, 127, e2022JB025009. https://doi.org/10.1029/2022JB025009

- Mousavi, N., Ardestani, V.E., 2023, 3D map of surface heat flow, low-temperature basins and Curie point depth of the Iranian plateau: Hydrocarbon reservoirs and iron deposits, Journal of the Earth and Space Physics, 48(4), 137-150. https://doi.org/10.22059/jesphys.2023.348000.1007453

Curie depth (Mousavi & Ardestani, 2023)

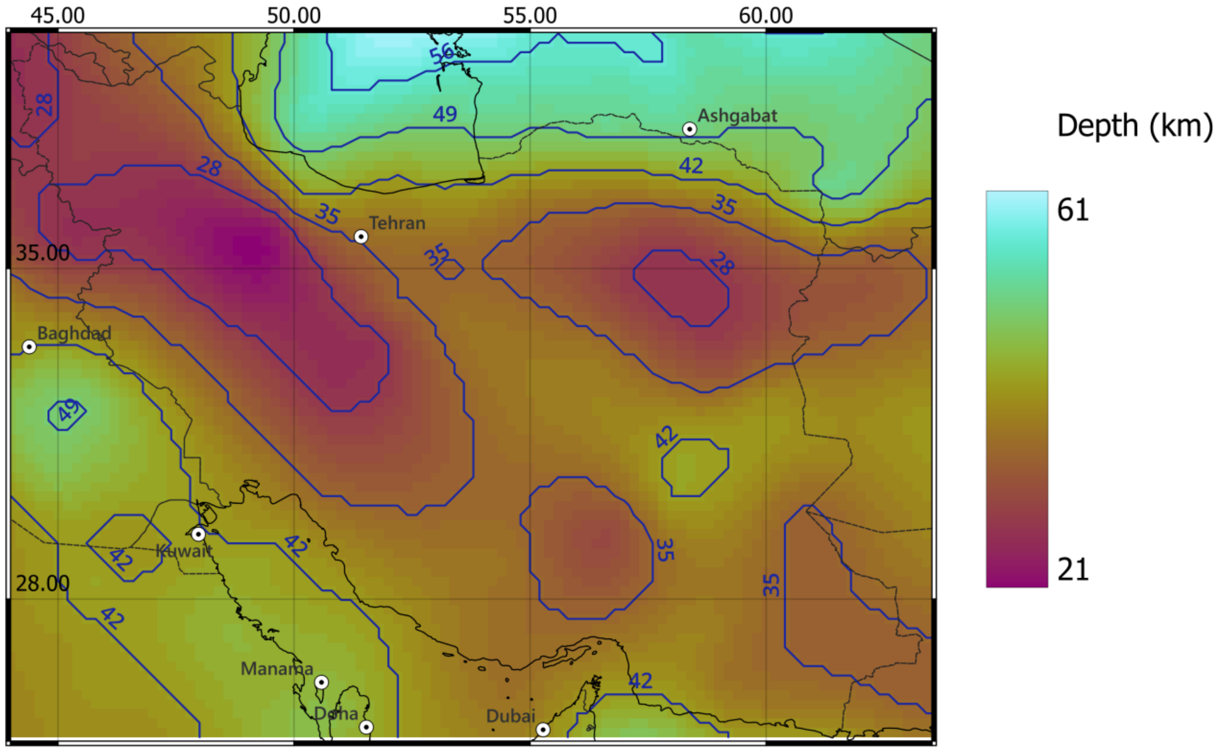

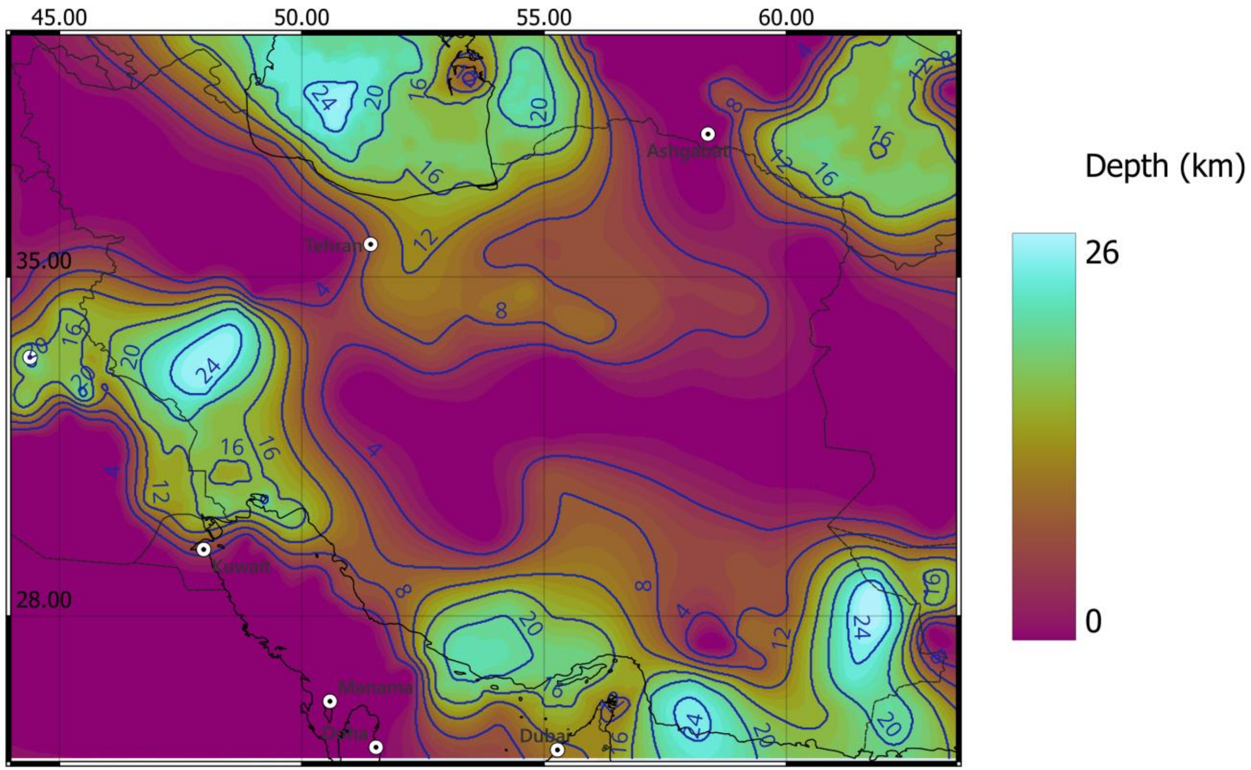

Sediment base depth (Irandoust et al., 2022)

Moho definition

Gradient Method (Tadiello & Braitenberg, 2021)

↓

Determination of the Moho depth studying the vertical velocity variations for each node.

↓

Research of the maximum vertical gradient, within a determined velocity range.

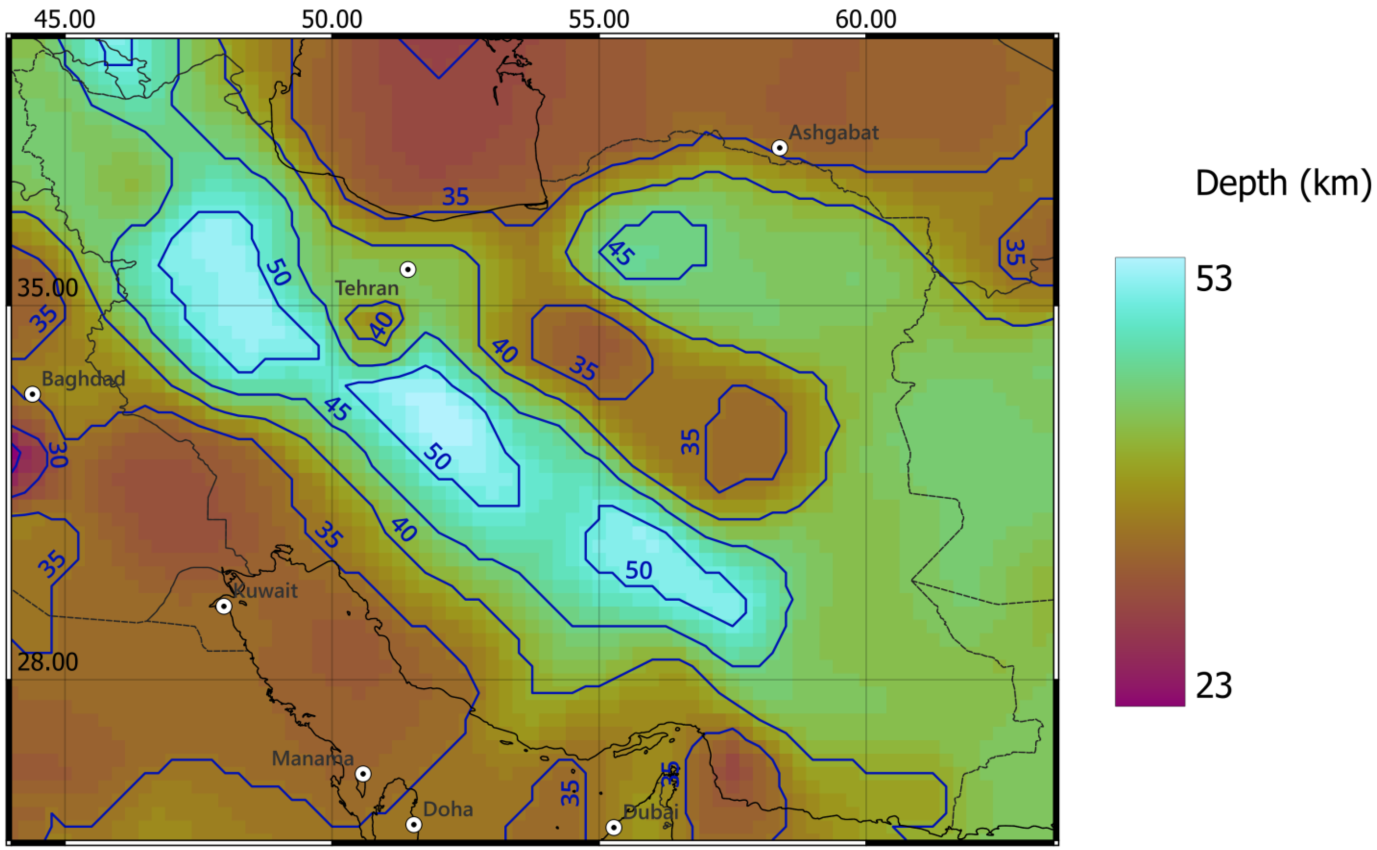

- Tadiello D. and Braitenberg C.; 2021: *Gravity modeling of the Alpine lithosphere affected by magmatism based on seismic tomography*. Solid Earth, 12(2), 539-561.

Density conversion

crust

Water: 2670 kg/m^3

Sediments / Cont. crust } Brocher's relation

$$V_p(km/s) = 0.9409 + 2.0947V_s - 0.8206V_s^2 + 0.2683V_s^3 - 0.0251V_s^4$$

$$\rho(g/cm^3) = 1.6612V_p - 0.4721V_p^2 + 0.0671V_p^3 - 0.0043V_p^4 + 0.000106V_p^5$$

mantle

Perple_X modeling

Na_2O	CaO	FeO	MgO	Al_2O_3	SiO_2	
0.13	1.90	7.90	41.60	2.00	45.20	(%)

Mantle velocities from tomography compared with synthetic upper mantle velocities and densities

- Thomas M. Brocher; Empirical Relations between Elastic Wavespeeds and Density in the Earth's Crust. Bulletin of the Seismological Society of America 2005;; 95 (6): 2081–2092. doi: https://doi.org/10.1785/0120050077

- Connolly, J. A. D. (2009), The geodynamic equation of state: What and how, Geochem. Geophys. Geosyst., 10, Q10014, doi:10.1029/2009GC002540.

Statistical inference

- Before applying Brocher's Equation, we try to simplify it with statistical inference.
- Applying Fischer's Law, we have demonstrated the possibility to delete the last term of the equation.

We found other parameters and defined a new relation for the V_p → density conversion:

$$\rho = 1,6026V_p - 0,4164V_p^2 + 0,0493V_p^3 - 0,0020V_p^4$$

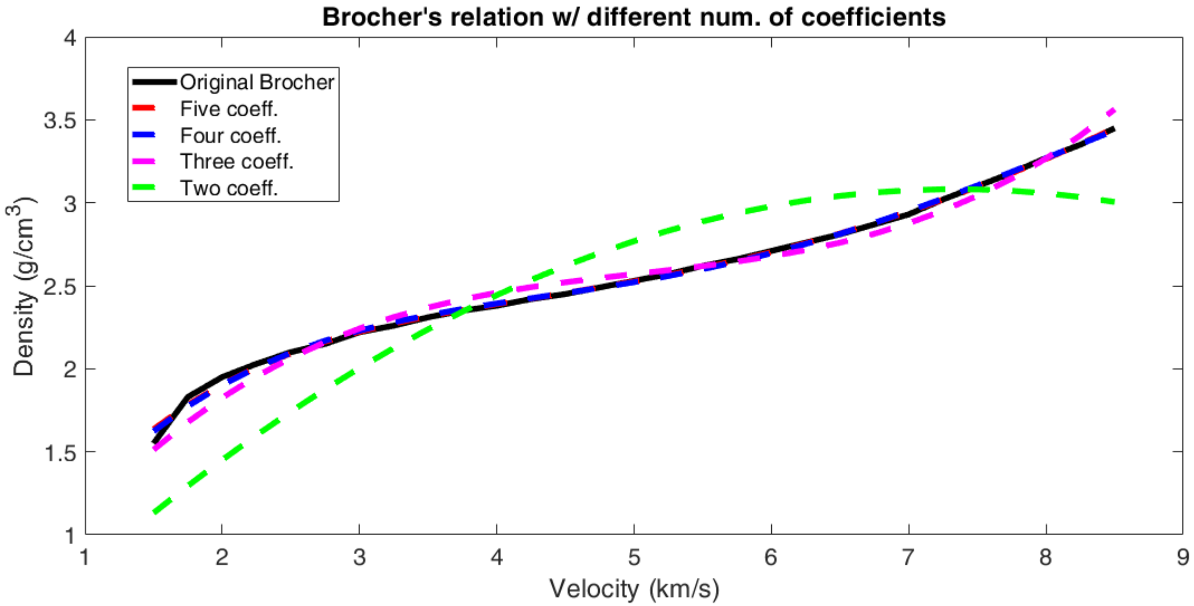

Results of the Brocher's relation (y-axis) with empirical velocity (x-axis) : Black line represent the original relation, dashed lines represent our test, starting from five coefficients and eliminating ones at every iteration.

Density inversion with Bayesian approach

- A probabilistic **Bayesian approach** is proposed for the joint gravity-magnetic inversion. It searches, from the a-priori model, the density distribution that minimizes the gravity and magnetic residuals.

$$P(\rho,\chi,\mathbf{L}|\Delta g^o,\Delta B^o) \propto \exp\Big\{-(\Delta g^o - \mathrm{A}_g\rho)^T \mathrm{C}_{\Delta g}^{-1}(\Delta g^o - \mathrm{A}_g\rho) - (\Delta B^o - \mathrm{A}_B\chi)^T \mathrm{C}_{\Delta B}^{-1}(\Delta B^o - \mathrm{A}_B\chi) - \\ - \frac{1}{\sigma^2_{\rho_\ell}}(\rho-\overline{\rho}_\ell)^2 - \frac{1}{\sigma^2_{\chi_\ell}}(\chi-\overline{\chi}_\ell)^2 - \gamma\sum_{i=1}^{N} s^2(L_i,\ell_i^o) - \lambda\sum_{i=1}^{N}\sum_{j\in\Delta_i} q^2(L_i,L_j)\Big\}\cdot \\ \cdot\, \delta_{[\overline{\rho}_\ell|3\sigma^2_{\rho_\ell}]}(\rho)\,\delta_{[\overline{\chi}_\ell|3\sigma^2_{\chi_\ell}]}(\chi)$$

- Marchetti, P., Sampietro, D., Capponi, M., Rossi, L., Reguzzoni, M., Porzio, F., Sansò, F. et al. (2019) *Lithological constrained gravity inversion. A Bayesian approach*. In: 81st EAGE Conference and Exhibition 2019. EAGE Publishing BV, 1–5

- Sansò, Fernando, and Daniele Sampietro. Analysis of the gravity field: Direct and inverse problems. Springer Nature, 2022.

- Sampietro, D., Capponi, M., Maurizio, G. (2022) *3D Bayesian Inversion of Potential Fields: The Quebec Oka Carbonatite Complex Case Study. Geosciences 2022, 12, 382. https://doi.org/10.3390/geosciences12100382*

- Thomas M. Brocher; Empirical Relations between Elastic Wavespeeds and Density in the Earth's Crust. Bulletin of the Seismological Society of America 2005;; 95 (6): 2081–2092. doi:https://doi.org/10.1785/0120050077

Elastic parameters calculation

- We use the final density model to calculate some elastic parameters.

$\boldsymbol{\mu = V_s^2 \rho}$ **(Shear modulus)**

$\lambda = \rho(V_p^2 - 2V_s^2)$ (1st Lame parameter)

$\sigma = \lambda/[2(\lambda + \mu)]$ (Poisson's ratio)

ρ_t= topo density = 2670 kg/m^3

Z_t= topo height

g= 9.81 m/s^2

Z= node depth

ρ= node density

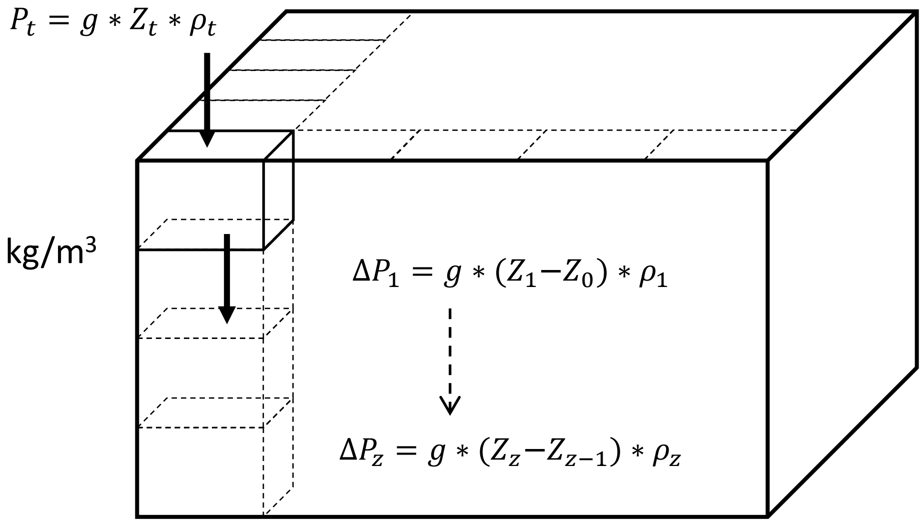

$$P = P_t + \sum_i^z \Delta P_i$$

Inversion results

- Field residuals

Magnetic

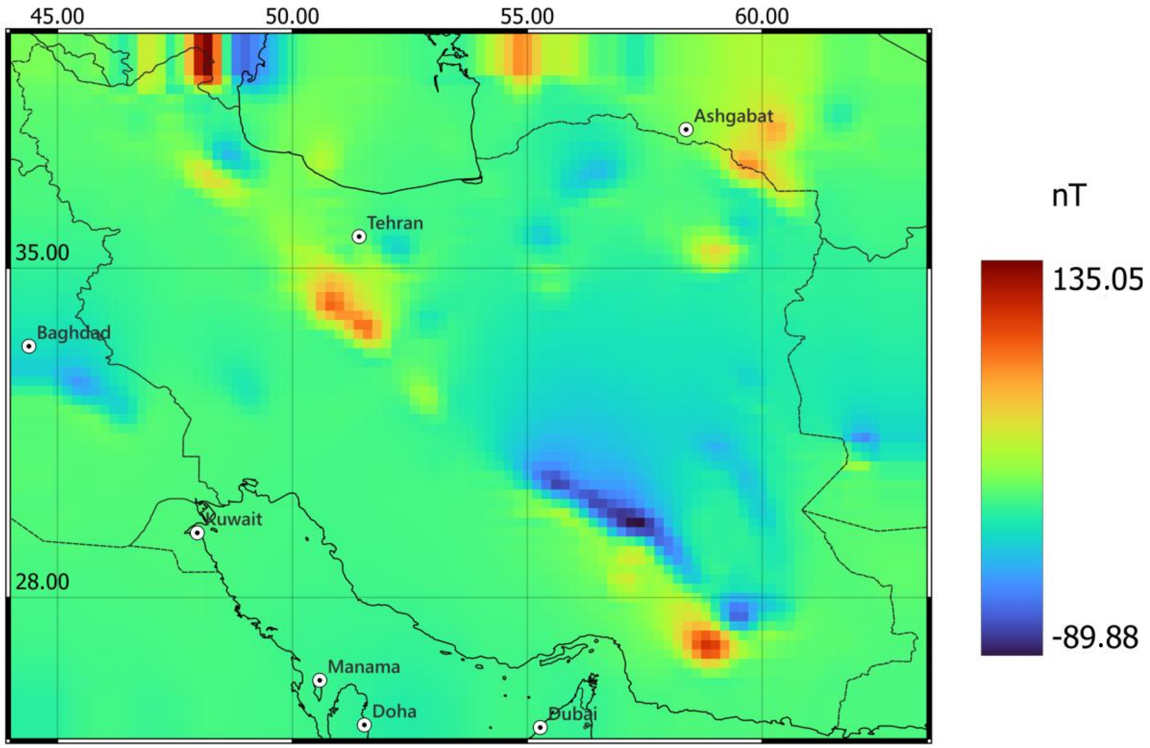

Std: 15 nT

Gravity

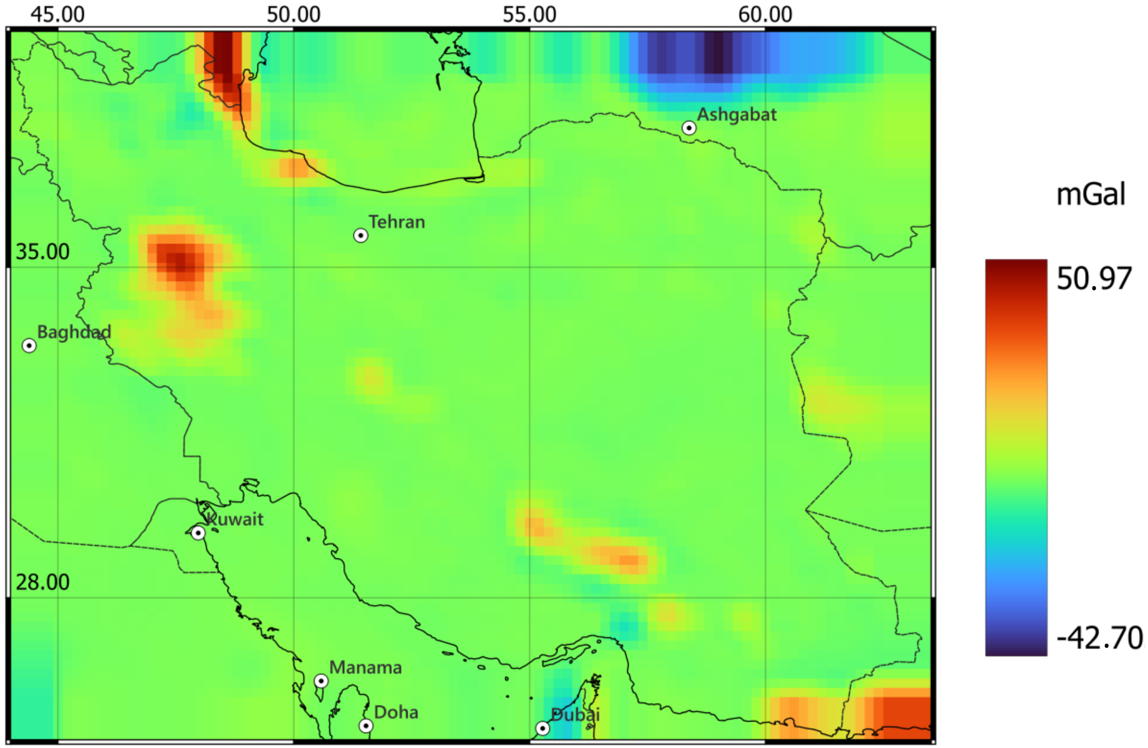

Std: 7 mGal

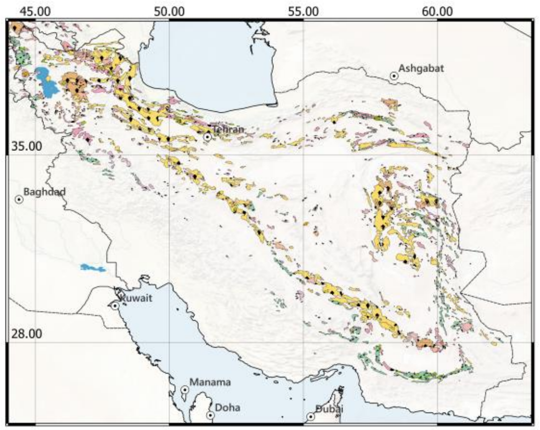

Discussion of inverted density

- Upper crustal density partly correlates with magmatic outcrops

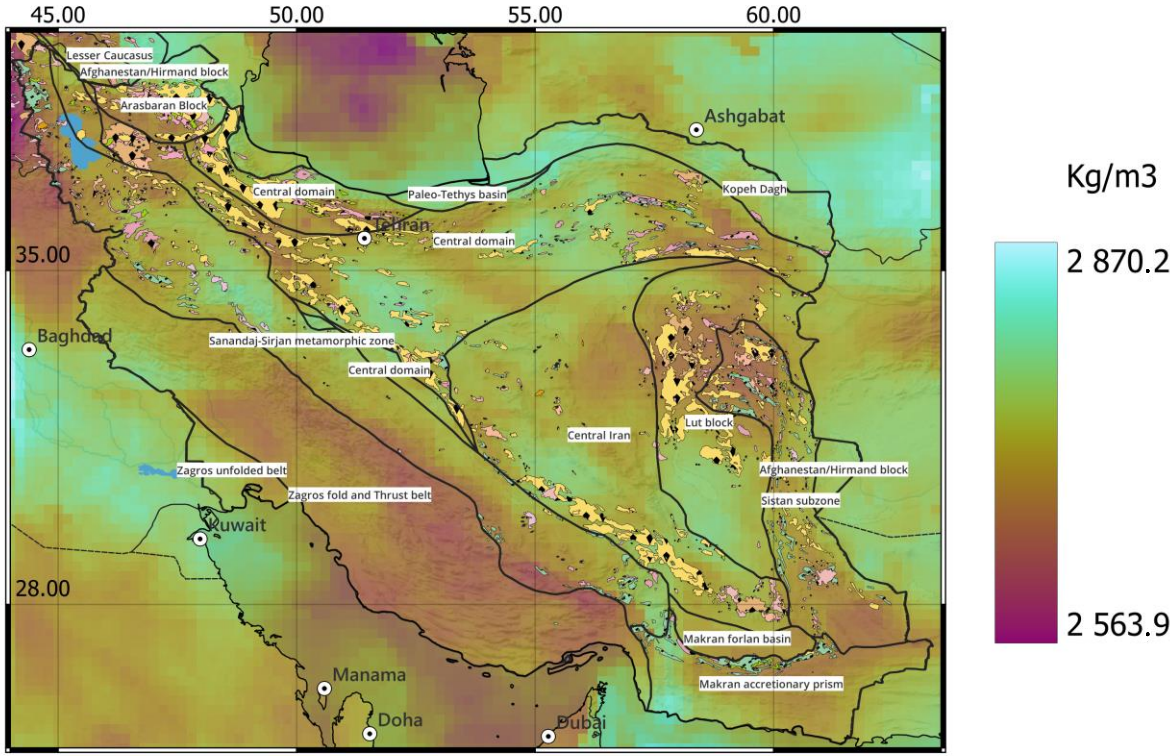

Crustal average density

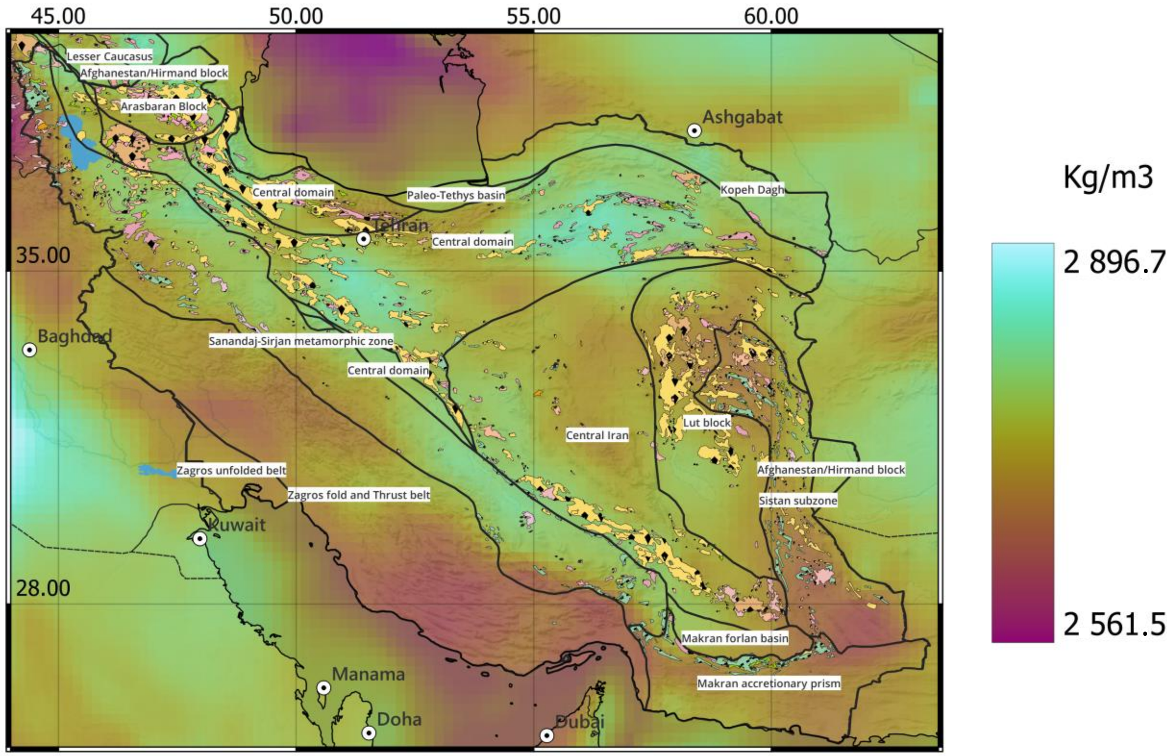

Depth: 20 km

Discussion of inverted density

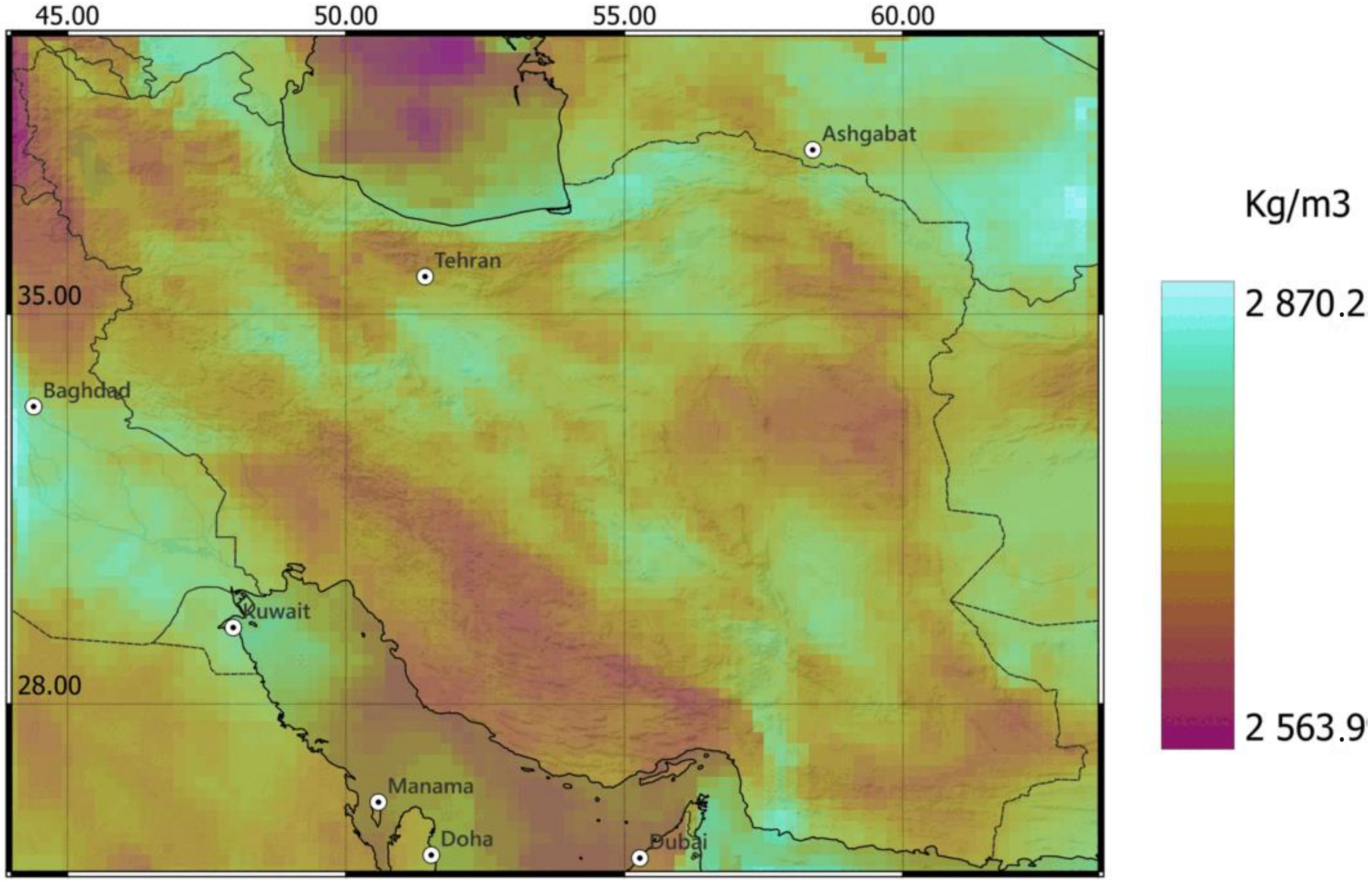

Crustal average density

- Lower crustal density vs Tethyan suture:

Paleo-Tethyan suture corresponds to a high-density trend.

Neo-Tethyan suture bounds a low-density area from an higher density zone

Lut Block focus

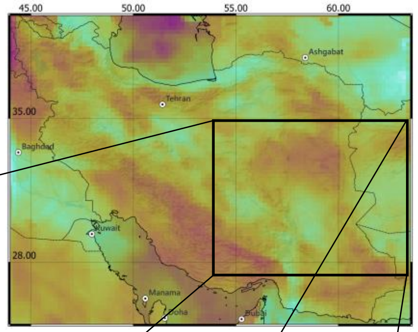

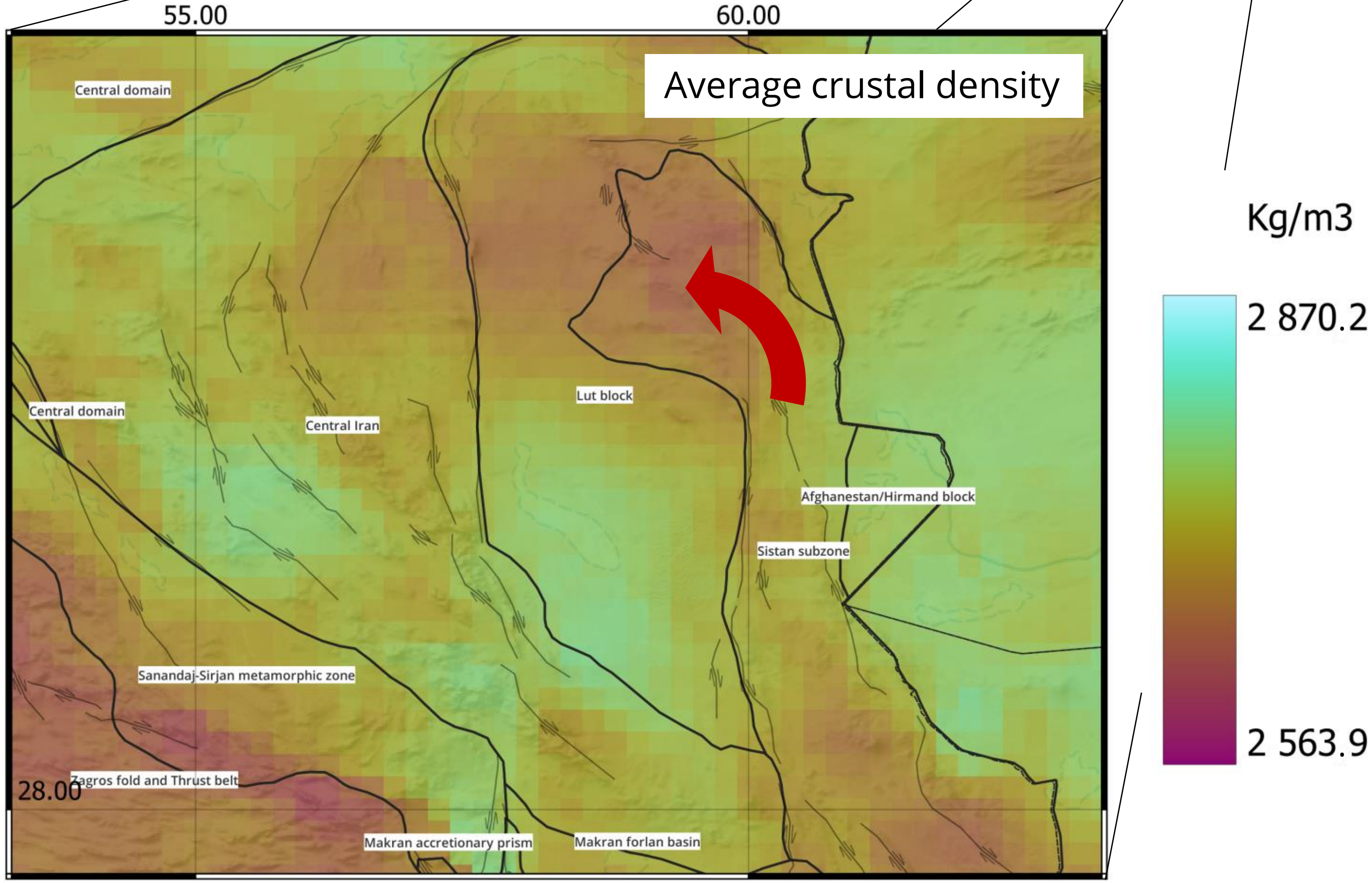

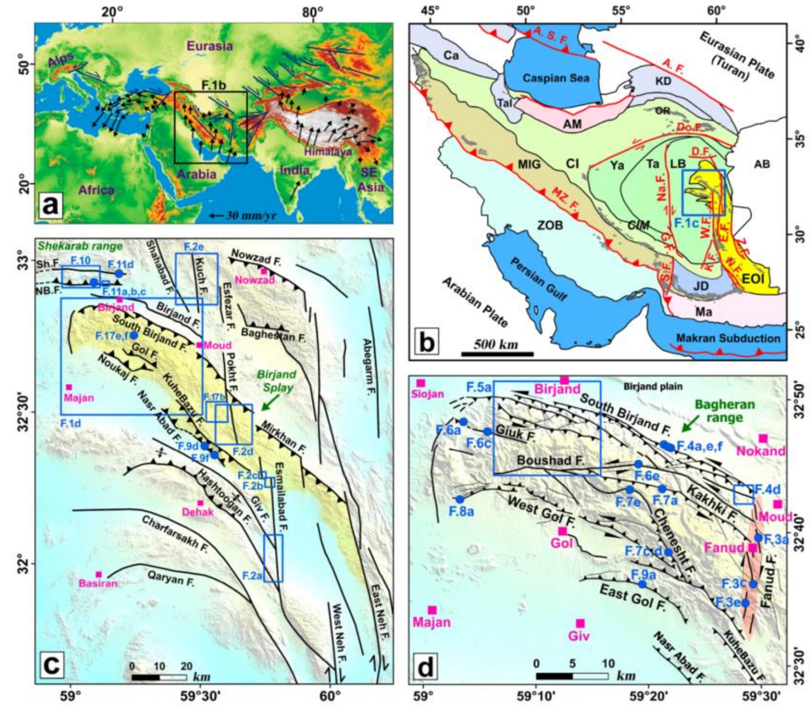

Tectonic of the area (from Rashidi et al., 2022)

- Density vs strike-slip faulting. Rotation of Birjand block helped by the presence of the high-density body.

- Rashidi, A., Shahpasandzadeh, M., Braitenberg, C., *Late Cenozoic to Present Kinematic of the North to Eastern Iran Orogen: Accommodating Opposite Sense of Fault Blocks Rotation*. Remote Sens. 2022, 14, 4048. https://doi.org/10.3390/rs14164048

Discussion of inverted susceptibility

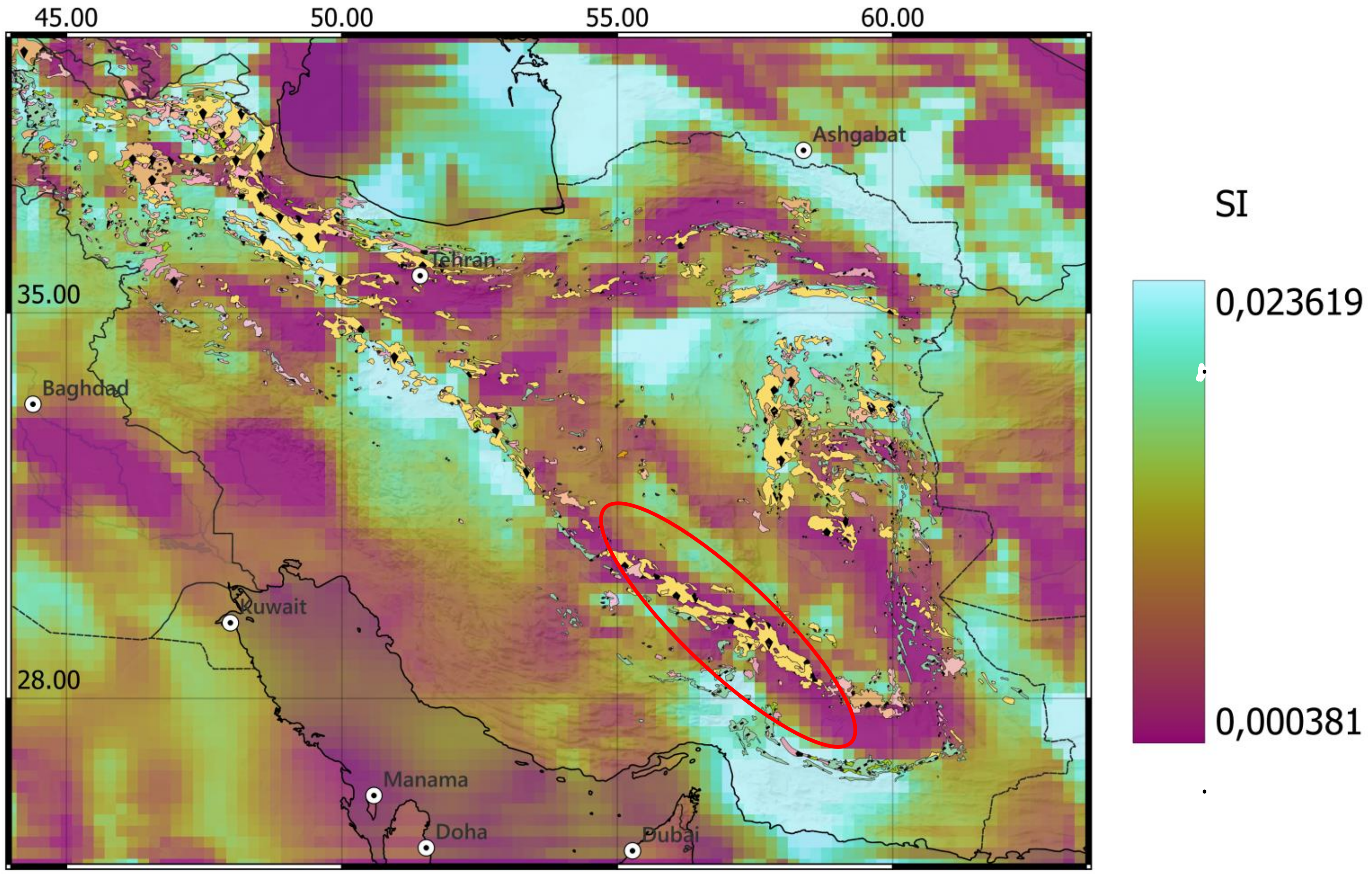

Crustal average susceptibility

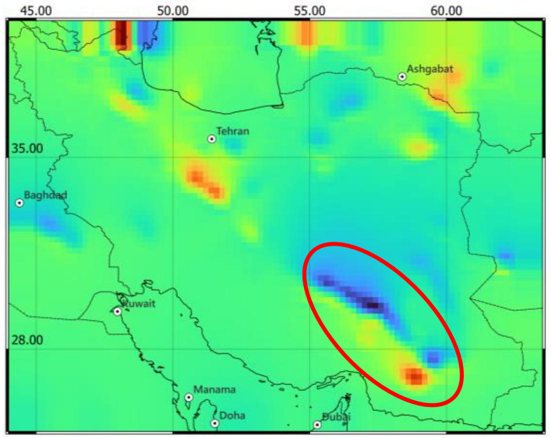

- High magnetization corresponds to west northwest presence of magmatic bodies.
- Highly magnetized body is detected in Central Iran and in Makran subduction zone.

Discussion of calculated shear modulus

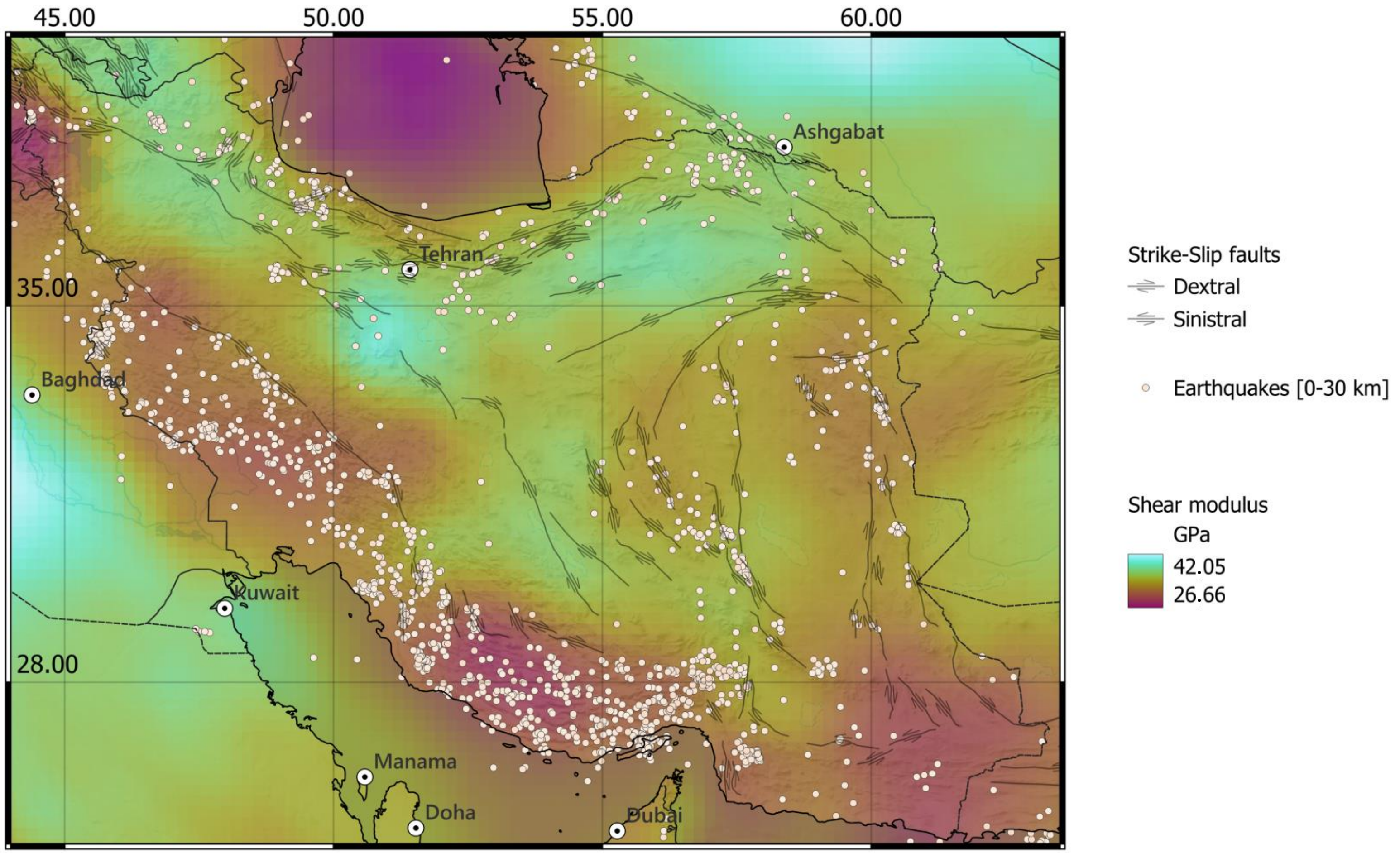

Depth: 20km

- Location of superficial earthquakes perfectly matches less rigid superficial areas.
- Exception is Caspian Sea. It is close to aseismic but has low rigidity.

Conclusion

- Bayesian joint gravity-magnetic inversion has defined a reliable 3D density and magnetic susceptibility model.

- The density variations match the geologically expected variations well.

- The seismic velocity and density has produced a rigidity model with significant variations. The more deformable areas are those with higher crustal seismicity.